

The AuScope Geodetic VLBI Array

J. E. J. Lovell · J. N. McCallum · P. B. Reid · P. M. McCulloch ·
B. E. Baynes · J. M. Dickey · S. S. Shabala · C. S. Watson · O. Titov ·
R. Ruddick · R. Twilley · C. Reynolds · S. J. Tingay · P. Shield ·
R. Adada · S. P. Ellingsen · J. S. Morgan · H. E. Bignall

Received: 22 August 2012 / Accepted: 18 February 2013

J. E. J. Lovell
School of Mathematics and Physics, University of Tasmania,
Private Bag 37, Hobart, 7001, Australia
Tel.: +61-3-6226-7256
Fax: +61-3-6226-2410
E-mail: Jim.Lovell@utas.edu.au

J. N. McCallum
School of Mathematics and Physics, University of Tasmania,
Private Bag 37, Hobart, 7001, Australia
Tel.: +61-3-6226-7529
Fax: +61-3-6226-2410
E-mail: Jamie.McCallum@utas.edu.au

P. B. Reid
School of Mathematics and Physics, University of Tasmania,
Private Bag 37, Hobart, 7001, Australia
Tel.: +61-3-6226-6383
Fax: +61-3-6226-2410
E-mail: Brett.Reid@utas.edu.au

P. M. McCulloch
School of Mathematics and Physics, University of Tasmania,
Private Bag 37, Hobart, 7001, Australia
Tel.: +61-3-6226-2420
Fax: +61-3-6226-2410
E-mail: Peter.McCulloch@inet.net.au

B. E. Baynes
School of Mathematics and Physics, University of Tasmania,
Private Bag 37, Hobart, 7001, Australia
Tel.: +61-3-6226-6383
Fax: +61-3-6226-2410
E-mail: Eric.Baynes@utas.edu.au

J. M. Dickey
School of Mathematics and Physics, University of Tasmania,
Private Bag 37, Hobart, 7001, Australia
Tel.: +61-3-6226-2447
Fax: +61-3-6226-2410
E-mail: John.Dickey@utas.edu.au

S. S. Shabala
School of Mathematics and Physics, University of Tasmania,
Private Bag 37, Hobart, 7001, Australia
Tel.: +61-3-6226-8502
Fax: +61-3-6226-2410

E-mail: Stanislav.Shabala@utas.edu.au

C. S. Watson
Surveying and Spatial Science Group, School of Geography
and Environmental Studies, University of Tasmania, Private
Bag 76, Hobart, 7001, Australia
Tel.: +61-3-6226-2489
Fax: +61-3-6226-7628
E-mail: Christopher.Watson@utas.edu.au

O. Titov
Geoscience Australia, P.O. Box 378, Canberra, ACT 2601,
Australia
Tel.: +61-2-6249-9064
Fax: +61-2-6249-9929
E-mail: Oleg.Titov@ga.gov.au

R. Ruddick
Geoscience Australia, P.O. Box 378, Canberra, ACT 2601,
Australia
Tel.: +61-2-6249-9426
Fax: +61-2-6249-9929
E-mail: Ryan.Ruddick@ga.gov.au

R. Twilley
Geoscience Australia, P.O. Box 378, Canberra, ACT 2601,
Australia
Tel.: +61-2-6249-9066
Fax: +61-2-6249-9929
E-mail: Bob.Twilley@ga.gov.au

C. Reynolds
International Centre for Radio Astronomy Research, Curtin
University, GPO Box U1987, Perth, WA 6845, Australia
Tel.: +61-8-9266-3785
Fax: +61-8-9266-9246
E-mail: c.reynolds@curtin.edu.au

S. J. Tingay
International Centre for Radio Astronomy Research, Curtin
University, GPO Box U1987, Perth, WA 6845, Australia
Tel.: +61-8-9266-3516
Fax: +61-8-9266-9246
E-mail: Steven.Tingay@icrar.org

P. Shield
InterTronic Solutions Inc., 452, Aime-Vincent, Vaudreuil-

Abstract The AuScope geodetic Very Long Baseline Interferometry array consists of three new 12 m radio telescopes and a correlation facility in Australia. The telescopes at Hobart (Tasmania), Katherine (Northern Territory) and Yarragadee (Western Australia) are co-located with other space geodetic techniques including Global Navigation Satellite Systems (GNSS) and gravity infrastructure, and in the case of Yarragadee, Satellite Laser Ranging (SLR) and Doppler Orbitography and Radiopositioning Integrated by Satellite (DORIS) facilities. The correlation facility is based in Perth (Western Australia).

This new facility will make significant contributions to improving the densification of the International Celestial Reference Frame in the Southern Hemisphere, and subsequently enhance the International Terrestrial Reference Frame through the ability to detect and mitigate systematic error. This, combined with the simultaneous densification of the GNSS network across Australia will enable the improved measurement of intraplate deformation across the Australian tectonic plate.

In this paper we present a description of this new infrastructure and present some initial results, including telescope performance measurements and positions of the telescopes in the International Terrestrial Reference Frame. We show that this array is already capable of achieving centimetre precision over typical long-baselines and that network and reference source sys-

tematic effects must be further improved to reach the ambitious goals of VLBI2010.

Keywords Geodesy · Very Long Baseline Interferometry (VLBI) · Celestial Reference Frame (CRF) · Terrestrial Reference Frame (TRF)

1 Introduction and Background

The AuScope Very Long Baseline Interferometry (VLBI) array was constructed as part of the National Cooperative Research Infrastructure Strategy (NCRIS) funded by the Australian Department of Innovation, Industry, Science, and Research (NCRIS 2006). The VLBI array is one part of AuScope, a diverse framework of infrastructure for research in geological, geochemical, geophysical, and geospatial subjects (AuScope 2012). The geospatial component of AuScope is composed of four kinds of infrastructure: the VLBI array, a suite of upgrades to Satellite Laser Ranging (SLR) facilities, a continent-wide array of ~ 100 Global Navigation Satellite Systems (GNSS) ground stations, and a number of precision gravity measurement instruments. These facilities work together, and in cooperation with similar equipment throughout the world, to define and monitor the geodetic reference frame and enable the improved geophysical interpretation of space geodetic data.

Various reference systems may be defined to form the foundation to realise a Terrestrial Reference Frame (TRF) which can be used to express positions on the Earth's dynamic surface (Petit and Luzum 2010). The space geodetic technique of VLBI provides a vital contribution to the realisation of the International TRF (ITRF2008, Altamimi *et al.* 2011), particularly through its ability to define the scale of the frame and its orientation with respect to the International Celestial Reference Frame (ICRF2, Fey *et al.* 2009). Observations with the VLBI technique uniquely define the inertial ICRF and continue to maintain and improve its precision.

The Earth Orientation Parameters (EOPs) are used to link the ICRF and ITRF and comprise five components: two nutation angles, two of polar motion and Universal Time (UT1). While other space-geodetic techniques (e.g. GNSS, SLR) provide information on polar motion, VLBI has capability of measuring all five EOPs and is unique in its ability to obtain the nutation angles and UT1. Therefore the ICRF2 as a realisation of the International Celestial Reference System (ICRS) must be carefully supported and maintained. See Schuh and Behrend (2012) for a review of the VLBI technique and its important contribution to geodesy.

Precise data on nutation is important in its own right as a probe of angular momentum changes in the

Dorion, Quebec, Canada, J7V 5V5
 Tel.: +1-450-424-5666
 Fax: +1-450-424-6611
 E-mail: pshield@intertronicsolutions.com

R. Adada
 Cobham Antenna Systems, SATCOM Land, 1551 College Park Business Center, Orlando, FL 32804, USA
 Tel.: +1-407-650-9054 ext.101
 Fax: +1-407-650-9086
 E-mail: Rami.Adada@cobham.com

S. P. Ellingsen
 School of Mathematics and Physics, University of Tasmania, Private Bag 37, Hobart, 7001, Australia
 Tel.: +61-3-6226-7588
 Fax: +61-3-6226-2410
 E-mail: Simon.Ellingsen@utas.edu.au

J. S. Morgan
 International Centre for Radio Astronomy Research, Curtin University, GPO Box U1987, Perth, WA 6845, Australia
 Tel.: +61-8-9266-9105
 Fax: +61-8-9266-9246
 E-mail: john.morgan@curtin.edu.au

H. E. Bignall
 International Centre for Radio Astronomy Research, Curtin University, GPO Box U1987, Perth, WA 6845, Australia
 Tel.: +61-8-9266-9245
 Fax: +61-8-9266-9246
 E-mail: h.bignall@curtin.edu.au

atmosphere, oceans, and interior of the Earth (e.g. Herring *et al.* 2002). Importantly, other space geodetic techniques including GNSS that densify the ITRF, depend upon frequent updates to the EOPs, in particular UT1 and precession/nutation, as determined through VLBI observations. These estimates are used a-priori and are often tightly constrained in order to achieve precise positioning over the Earth. Combined, this is the mission of the International VLBI Service (IVS) for Geodesy and Astrometry (Schuh and Behrend 2012).

The 26 m telescope at the Mt. Pleasant Observatory of the University of Tasmania, near Hobart, has been a member of the IVS network and its predecessors for more than 20 years. Hobart is one of the few IVS network sites in the Southern Hemisphere that can work all year round and is able to contribute its data rapidly to the IVS correlation centres in North America and Europe. As of 2006, the only IVS observatories at mid to high southern latitudes capable of frequent, year-round observations were in Chile (the Transportable Integrated Geodetic Observatory (TIGO)), South Africa (Hartebeesthoek Radio Astronomy Observatory), and Hobart. In order to expand the ability of the IVS to monitor ICRF sources south of declination -40° , it was very important to increase the number of telescopes at southern latitudes (Titov 2009). Thus one of the major objectives of the AuScope infrastructure strategy was to build three new VLBI telescopes in Australia. The physical positioning of the telescopes seeks to optimise the possible improvements to the ICRF and ITRF from the Australian continent (Figure 1). The GNSS array then provides the densification required to achieve the goal of enabling high precision coordination across the continent.

The three new AuScope VLBI antennas are located at Hobart (Tasmania), Katherine (Northern Territory) and Yarragadee (Western Australia) (Figure 1). The new Hobart telescope is co-located with the existing 26 m telescope to preserve the more than 20 year VLBI time series at the site. Midway between the 26 m and 12 m telescopes is the HOB2 GNSS installation which has been a core site of the International GNSS Service (IGS) since its inception. A hut capable of housing a mobile gravimeter is also co-located on the site. The Yarragadee telescope provides a far western point on the continent and is co-located with multiple existing geodetic techniques including SLR, GNSS, Doppler Orbitography and Radiopositioning Integrated by Satellite (DORIS) and gravity. The Katherine site is new and provides a central longitude, northern site. The telescope is co-located with a new GNSS site that forms part of the AuScope GNSS network.

The design of the new AuScope telescopes was driven by a new paradigm for the IVS, defined by a study team in the early 2000's and given the name VLBI2010 (Niell *et al.* 2007; Petrachenko *et al.* 2010). A critical specification for the new telescope design is drive speed. This provides better performance for the specific needs of a geodetic VLBI array because it allows the telescopes to observe more sources at wide separations on the sky in a given time interval (Titov 2007). Rapid switching from source to source is a critical telescope design parameter in order to solve for the effects of the troposphere on the propagation delay of the radio signals. With this in mind, the VLBI2010 model favours small telescopes (12 m rather than ~ 25 m diameter) with powerful drive motors.

Each AuScope VLBI observatory is equipped with a 12.1 m diameter main reflector designed and constructed by COBHAM Satcom, Patriot Products division. All sites are equipped with dual polarization S and X-band (2.2 – 2.4 GHz and 8.1 – 9.1 GHz respectively) feeds from COBHAM with room temperature receivers developed at the University of Tasmania by Prof. Peter McCulloch. Data digitisation and formatting is managed by the Digital Base Band Converter (DBBC) system from HAT-Lab, and data are recorded using the Conduant Mark5B+ system. Each site is equipped with VCH-1005A Hydrogen maser time and frequency standards from Vremya-CH.

The AuScope infrastructure funding also included an allocation to establish a software correlator, the Curtin University Parallel Processor for Astronomy (CUPPA), a 20 node beowulf compute cluster running the DiFX software correlator (Deller *et al.* 2011) to process data from the array.

In this paper we provide a detailed description of the telescopes and associated hardware, signal processing, control and monitoring equipment and the correlation facility. Lastly, we describe the performance of the telescopes and present some initial geodetic results from the array.

2 The Observatories

2.1 Antenna Characteristics

The 12 m cassegrain shaped reflector, pedestal mounted antennas (Figure 2) are of a unique design in this size range as they use a large ball jack screw permanently in compression for elevation. This elevation drive therefore uses just one motor as backlash is taken care of by keeping the jack in compression. For azimuth however two motors and pinions are used on the main azimuth

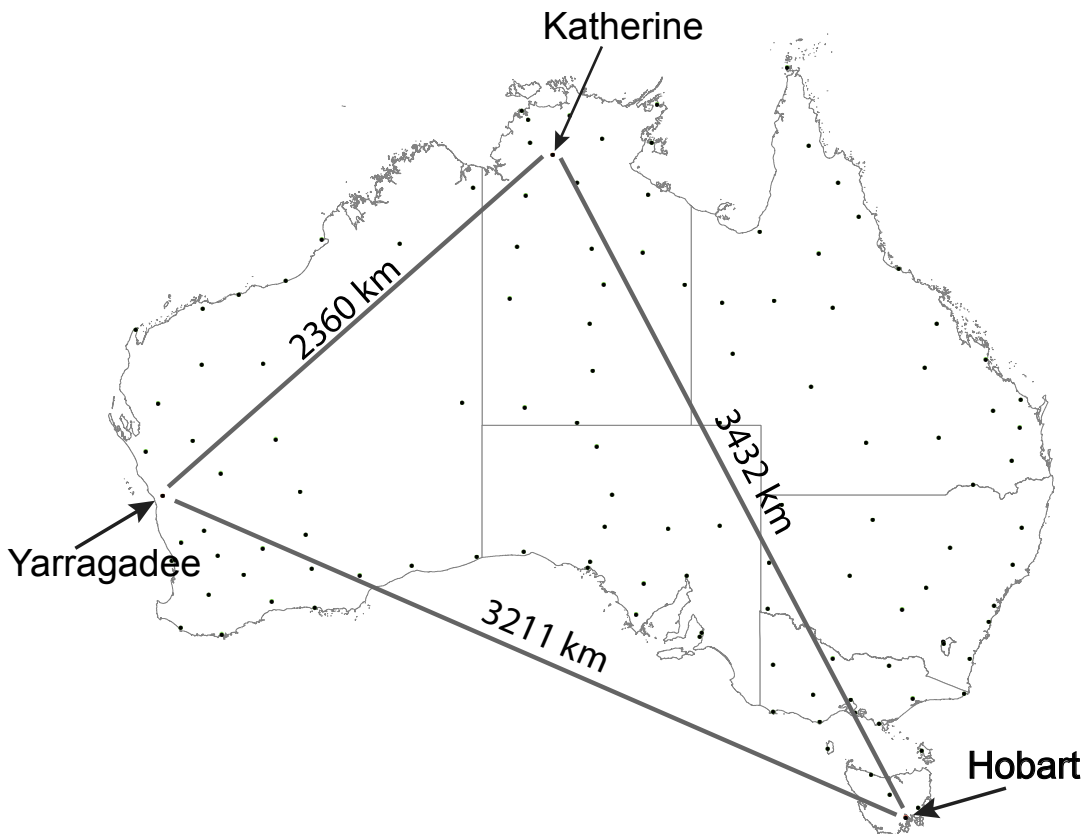


Fig. 1 The geographical distribution of VLBI and GNSS infrastructure for AuScope. The locations of the new 12 m telescopes are labelled and the new GNSS sites are indicated by filled dots.

gear/bearing and the motors are electrically torque biased against each other to eliminate any backlash. The motors are high torque standard AC brushless servo motors and two stages of gearbox reduction are used on both axes to increase the torque and reduce speed. The main azimuth gear/bearing is a massively oversized, nearly 2.3 m diameter, opposing roller bearing system ensuring great precision and long life.

The combination of materials used in the antenna is somewhat unconventional. The primary reflector, including its shape-determining support ribs, hub etc are aluminium but below the elevation bearings the whole turning head and pedestal are made of steel, and painted for thermal and corrosion prevention. The subreflector is a custom shaped carbon fiber reinforced polymer moulding.

The main 12 m reflector is fabricated with water jet cut radial ribs that determine the final surface 0.38 mm RMS shape, a rigid aluminium hub, stretch formed precision front reflector panels and rear close out panels. The stretch formed panels need to be attached to the

ribs to hold their shape, and the rear close out panels strengthen the radial ribs. Once the main reflector is fully assembled and locked up tight it is a strong structure. However, there is essentially no individual panel surface adjustability.

The antenna can slew at up to 5 deg/s in azimuth and 1.5 deg/s in elevation. The control system monitors and controls the whole system using 26 bit optical absolute position feedback devices mounted right on the axes of motion. The RFI-tight control system utilises standard modern COTS servo systems and components. The control software was developed under contract by Dr. Mark Godwin in the UK.

2.2 Telescope optics and feed

The COBHAM Satcom 12 m antenna system was jointly developed with NASA's Jet Propulsion Laboratory as part of the proof of concept for the Deep Space Networks large array proposal (Gatti 2004). The radio frequency optical design of the system (based on the work

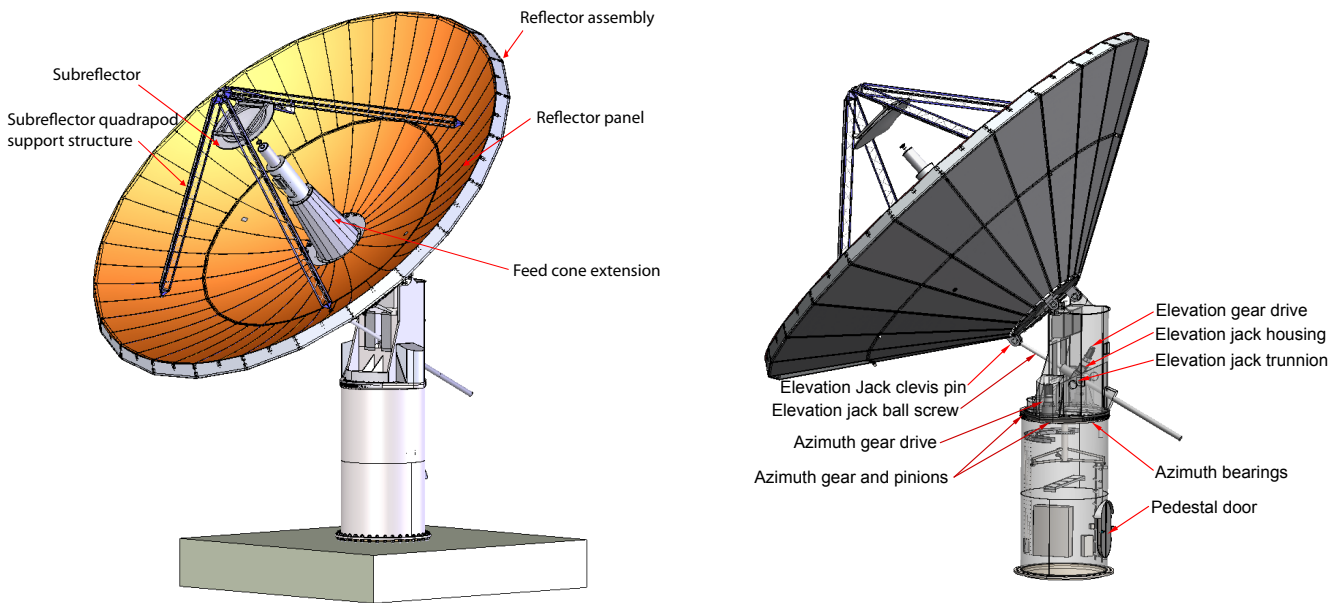


Fig. 2 Drawings of the antennas used in the AuScope VLBI array with the main components labeled.

presented in Imbriale 2005) utilises a shaped Cassegrain configuration optimised for maximum G/T performance with a 1.8 m subreflector.

The feed for the antenna system, developed by COBHAM in response to interest from the radio astronomy community, employs a 4-port coaxial configuration to allow for simultaneous reception of right- and left-hand circular polarisation signals (RCP and LCP respectively) at both the S and X bands. The feeds operating frequency ranges are 2.2–2.4 GHz at S-Band and 8.1–9.1 GHz at X-Band. A cross section diagram of the feed is presented in Online Resource 1 (Figure 3). A breakdown of the expected system performance is tabulated in Online Resource 2 (Table 1) but can be summarised by System Equivalent Flux Densities (SEFDs) of 3500 Jy and 3400 Jy at S- and X-bands respectively.

2.3 Front end receiver (feed tube and hub)

The receiver takes the dual circular polarisation signals from Low Noise Amplifiers (LNA) on the feed, each with ~ 35 dB of gain, and down-converts them to baseband suitable for detection and further processing. Figure 4 provides an overview of the signal path,

a description of which follows in this and the next two Subsections.

The receiver allows for injection of calibration signals from noise diodes, a tone generator and/or a separate phase-calibration pulse generator. Two noise diode signals may be injected: a low power signal (~ 0.1 dB) suitable for modulation to enable continuous system temperature (T_{sys}) measurements; or from a higher-powered signal (~ 0.5 dB) for single T_{sys} measurements or system testing. A tone injection port is available for coherence testing or other maintenance and configuration tasks.

In the situation where only a single polarisation is required (as is common in current geodetic VLBI observations or spacecraft tracking applications) some redundancy is provided by cross-over switches in the signal path to permit quick swapping of polarisations. This allows for continued operation in the event of a component failure downstream of the switches.

The receiver has front-end filters which pass through 2.0 to 2.5 GHz at S-band and 8.0 to 9.2 GHz at X-band. The receiver system also permits inclusion of notch filters to block interference signals prior to down-conversion.

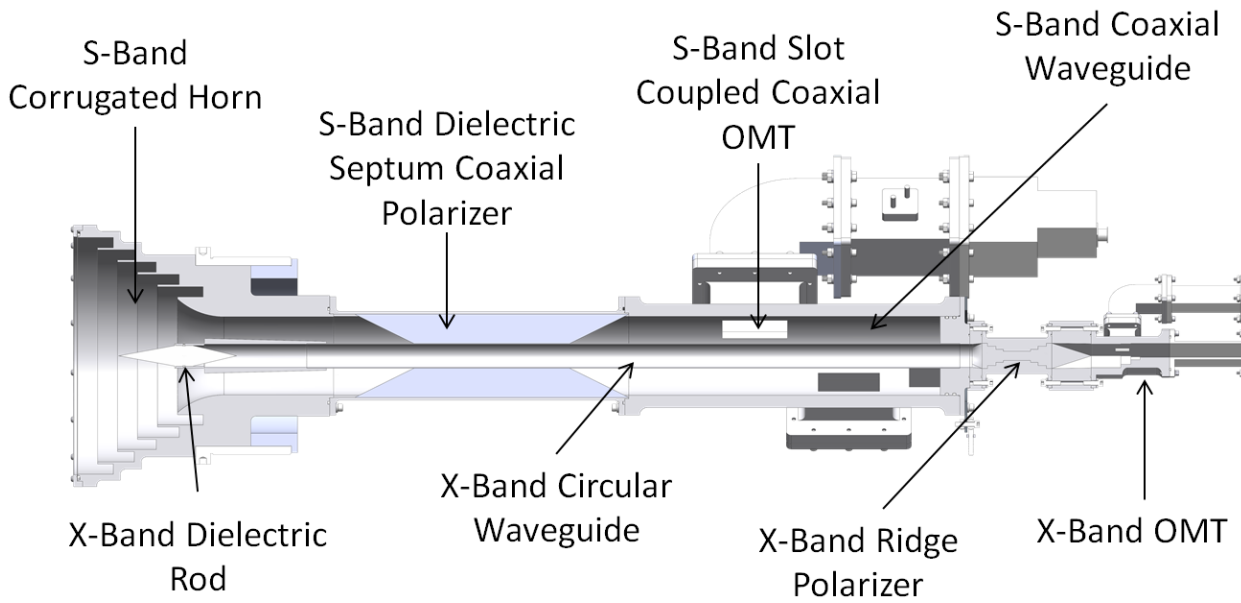


Fig. 3 Online Resource 1: A cross-sectional diagram of the coaxial S/X feed developed for the 12m antennas.

Table 1 Online Resource 2: Expected Performance of the 12m Radio Telescope with Dual Band S/X Feed

| | Parameter | S Band | X Band | Additional Notes |
|--------------------------|-----------------------------------------------------|--------|--------|----------------------------------------------------|
| Losses | Spillover & Illumination loss (dB) | 0.81 | 0.66 | i.e. 83% and 86% efficiency respectively |
| | Blockage Loss (dB) | 0.71 | 0.71 | Blocked aperture due to Subreflector and Quadripod |
| | VSWR Loss (dB) | 0.14 | 0.04 | < -15 dB and -20 dB Return Loss |
| | Port to Port Isolation (dB) | 0.04 | 0.04 | > 20 dB isolation |
| | Cross-polarisation loss (dB) | 0.03 | 0.03 | Axial Ratio < 1.5 dB |
| | Surface RMS Loss (dB) | 0.01 | 0.09 | Using Ruze equation and RMS of 0.38 mm |
| | Ohmic Losses (dB) | 0.5 | 0.35 | In Window, Horn, Polarizer and OMT |
| | Total Loss (dB) | 2.24 | 1.92 | |
| | Total Aperture Efficiency | 59.7% | 64.3% | |
| Noise Temperature | LNA (K) | 30 | 50 | Manufacturer Specification |
| | Feed (K) | 35 | 25 | Based on Ohmic losses above at 290 K |
| | Quadripod, Subreflector and S-Band Horn Scatter (K) | 10 | 5 | |
| | Galactic + Atmospheric (K) | 10 | 10 | |
| | System Noise temperature (K) | 85 | 90 | |
| Sensitivity | SEFD (Jy) | 3500 | 3400 | |

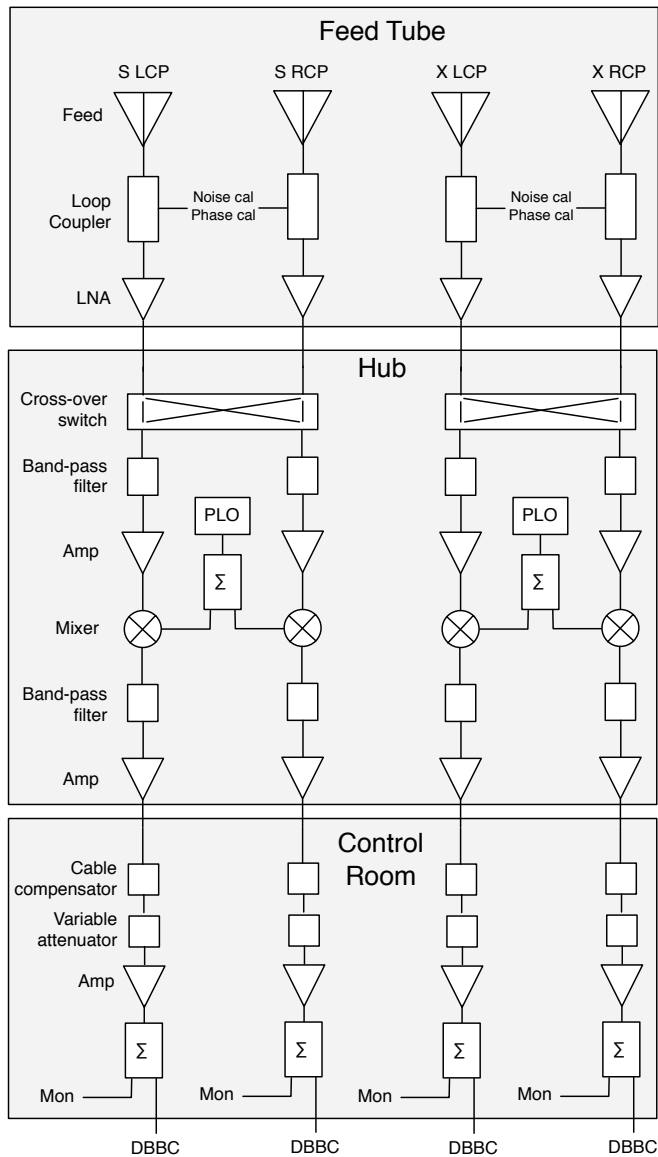


Fig. 4 A schematic, illustrating the signal path from the feed at the focal point to the receiver in the antenna hub (immediately below the feed cone extension labeled in Figure 2) to the IF signal outputs to the DBBC.

The front-end receiver down-converts the S- and X-band signals with local oscillators at 1900 MHz and 7600 MHz respectively, phase-locked to a 100 MHz tone from the hydrogen maser.

2.4 Back end receiver and recorder (control room)

The down-converted signals from the front end receiver are then carried underground to the control room where an Intermediate Frequency (IF) unit provides some signal conditioning to bring output power levels into range, then into the DBBC for sampling. The sampled data are then recorded to disk using a Mark5B+ unit.

The IF unit consists of 4 signal chains (RCP and LCP of S- and X-band), each with tuned cable compensators, IF amplifiers and independent controllable attenuator arrays. The outputs of each IF are split with two outputs going to the inputs of the DBBC conditioning modules, together with one other output as an analogue monitor point. In normal operation, these monitoring points are connected to a remotely controlled selector device which determines the input to a broad-band power sensor. A network-accessible spectrum analyser is also connected to this analogue monitor point. This is particularly useful for detecting the presence of interfering signals.

The DBBC system is composed of a series of modules which filter and sample the input IFs and produce a number of output baseband-converted channels. The IF selection and bandpass filtering is handled by the Conditioning Modules. These modules support up to 4 input IFs, and the selected IF can then be filtered by one of three selectable, 512 MHz wide, bandpass filters (in the ranges of 0–512, 512–1024 and 1024–1536 MHz). The total power level of the IF is then adjusted using variable attenuators within the Conditioning Modules before being sampled. The DBBC sampler is synchronised to the station maser through a 10 MHz and 1 pulse-per-second (1PPS) signal. There are four tuneable baseband converter units supplied from each of the 4 Conditioning Modules, which can provide up to 32 data channels (upper and lower sidebands). The channel selection for the output data stream is controlled by the DBBC. Currently, there are two channel mappings available - the standard geodetic format for S/X or the “VLBA” format which records the upper and lower sidebands of 8 channels. The data are written out at 2-bit resolution. With the selectable IFs and bandpass filters, all standard S/X geodetic observing modes are supported as well as those used for astronomical and astrometric observations.

The VLBI Data Interchange (VSI) format data stream from the DBBC is recorded using Mark5B+ recorders located at each site. A selectable bit-mask can be applied to the data stream to select a subset of channels for recording, and also the sampling quantisation. The Mark5B+ can support recording rates of up to 1 Gbps using a single Mark5 data module. The majority of experiments made using the AuScope antennas have been carried out at 256 Mbps (16 8 MHz channels with 1-bit quantisation) although 1 Gbps data rates (16 16 MHz channels with 2-bit quantisation) have been used successfully in some experiments.

The Mark5B+ recorder is responsible for the formatting of the recorded data. During the initialisation of the recorder, the Mark5B+ is synchronised to the

1PPS from the DBBC via the VSI interface. Thereafter, the 1PPS generator internal to the Mark5B+ is responsible for the timing, using the 32 MHz VSI clock as a reference. The Mark5B+ maintains an internal comparison between the input and synthesised 1PPS which can be checked via the control software. An output 1PPS is also synthesised by the Mark5B+ unit, and the offset between this and the station GPS receiver 1PPS is used as another way of measuring the timing stability of the system. The Mark5B+ is synchronised to the station's GPS-Clock for establishing the recording epoch.

2.5 Control and monitoring systems

Calibration signals, cross-over switches and IF Unit attenuation settings are all remotely controllable through a serial interface. This interface also permits monitoring of temperatures and voltages throughout the system.

All of the IF and recording systems are controlled by the PC Field System (PCFS) computer. The AuScope antennas use a standard PCFS configuration (the current 9.10.04 version) with customised modules for antenna control and system monitoring. The PCFS host machines are server-class machines using RAID file systems for reliability.

Control and monitoring of the experiments is carried out using the eRemoteControl interface for the PCFS, together with the Open-Monica system (MONICA 2011). eRemoteControl was developed by Neidhardt *et al.* (2010) and offers significant benefits in bandwidth usage and connection reliability for the remote sites. The Monica system collects information on the observing system from a number of monitoring points, including supply voltages for the receiver electronics, temperature and humidity in the antenna structure, wind conditions, drive parameters and important physical parameters such as external temperature, atmospheric pressure and relative humidity. Most of the analogue interfaces are provided by PICAXE-based devices which are interfaced to Monica via simple TCP servers.

All of the information collected by Monica is permanently logged to assist in post-facto fault finding. A real-time monitoring system is also present to detect any faults when they occur, and to warn the operator.

3 The Correlator

Following the observations, data from each station are sent to a correlator for processing. The correlator essentially replays the observation, combining telescope signals to provide the fundamental measurement of geodetic VLBI: the time delays in signal arrival between an-

tennas on a baseline-by-baseline basis. Until recently, the need to process the large volumes of raw data from observatories has required purpose-built hardware correlators. However, the advent of fast, inexpensive multi-core computer processors and high bandwidth networking has permitted the development of flexible and scalable software-based correlators such as the DiFX correlator (Deller *et al.* 2007, 2011).

The correlator runs on the AuScope-funded Curtin University Parallel Processor for Astronomy (CUPPA). The correlator hardware consists of a 20 node beowulf cluster, currently with approximately 90 TB of attached storage, installed at, and operated by, Curtin University in Perth, Western Australia. The individual nodes each contain dual quad-core 2.66 GHz Intel Xeon CPUs, 8 GB of RAM and have Gigabit ethernet connectivity. The correlator is connected by a 10 Gigabit ethernet connection to iVEC (the Western Australian supercomputing centre) allowing transfer of data from remote stations via the internet without the necessity of shipping disks.

The correlator software is the latest release version of DiFX, run under a locally developed data management software system. Data quality is checked using a pipeline system, also developed at Curtin University, which utilises the ParseTongue (Kettenis *et al.* 2006) interface to NRAO's AIPS radio astronomy data analysis software. It is also possible to export the data to HOPS (Haystack Observatory Postprocessing System) for further quality assessment and data reduction.

This combination of hardware and software is capable of processing a standard AuScope experiment (up to 4 stations, each recording at 256 Mbps) in approximately 30% of the observation time.

DiFX is rapidly becoming the standard correlator for geodetic VLBI. It is used exclusively at Curtin, at the VLBA correlator in Socorro and at the Bonn software correlator. It is also used for geodetic VLBI processing at the IVS correlation facilities at Washington and Haystack. All of these facilities are actively involved in the development of DiFX for geodesy and astronomy. This active development means that it is compatible with a wide range of back-ends and recording systems.

DiFX has been tested against a trusted geodetic correlator (Tingay *et al.* 2009). Tests have been developed to ensure consistency between versions of the correlator (Deller *et al.* 2011). Further verification of consistency of Geodetic and Astrometric observables is underway (Morgan and Petrov in preparation). DiFX is fully scalable. As an example, the current CUPPA cluster is more than capable of correlating a 10-station 4 Gbps experiment (albeit slower than real time).

4 Observations and Operations

Construction of the first AuScope telescope at Hobart was completed in 2009 and officially opened at the IVS General Meeting on 9 February 2010. Following a period of commissioning, testing and debugging, the Hobart telescope made its first successful IVS observation in October 2010. Construction and commissioning at the other two sites continued in parallel. Yarragadee made its first successful IVS observation in May 2011 and, following a successful full-network fringe check on 8 June 2011, correlated at Curtin University, all three telescopes participated in an IVS observation for the first time on 16 June 2011.

To keep operating costs at a minimum, all three observatories were designed and constructed to be remotely controlled and monitored. Operation of the AuScope VLBI array is being carried out from a dedicated operations room on the Sandy Bay campus of the University of Tasmania. Typically a single operator will control and monitor the observations with a local person at each of the sites available on-call when manual intervention is required. At the end of a session, recorded media are sent to the designated correlation facility by courier in the case of Yarragadee and Katherine but at Hobart the data are transferred electronically via a fast network connection.

At present, the AuScope VLBI facility has sufficient operational funds for ~ 70 observing days per year, usually consisting of two AuScope telescopes observing as part of the IVS network. Unfortunately operational funds are not presently sufficient to support correlation at Curtin University, so all data are sent to the IVS correlation facilities at Bonn (Germany), Washington (USA) or Haystack (USA).

5 Initial Results

5.1 Antenna Performance

During the commissioning of the antennas and after any work on the receiver system, the system temperature is measured by comparing total output power levels with and without a microwave absorber placed over the feed horn. Assuming an LNA effective temperature of 30 K at S-band and 50 K at X-band, the inferred system temperature is generally in the range of 85–90 K for a system in good order. The system temperature at the Hobart telescope is currently slightly elevated at S-band (95 K). The exact cause of this increase is under investigation but a slight misalignment in the waveguide is suspected. The SEFD of the telescope was estimated using sources from the Ott *et al.* (1994) catalogue as

flux density calibrators, primarily Virgo A and Hydra A. The zenith SEFD of the AuScope antennas is estimated at ~ 3500 Jy for both S- and X-band, in good agreement with the predicted values. Measurements of SEFD as a function of elevation at S- and X-band are shown in Figure 5.

The gain of the telescope was measured using observations of sources that transited near to the zenith. The amplitude of the sources relative to the noise diode was measured at elevations between 10 and 85 degrees. At S-band, there is no evidence for any change with respect to elevation with an estimated aperture efficiency of 60%. At X-band, the optimal gain is seen at an elevation of 55 degrees and a slight decrease is apparent toward the zenith and horizon. The peak aperture efficiency is 64%, decreasing to 60% at the zenith. The estimated values of the system temperature and aperture efficiency are in good agreement with the predicted values for both S- and X-band. The X-band aperture efficiency as a function of elevation (in degrees) was estimated via a polynomial fit (Figure 6) which is:

$$A(\text{El}) = -2.77 \times 10^{-5} \text{El}^2 + 3.03 \times 10^{-3} \text{El} + 0.555 \quad (1)$$

The pointing model is currently implemented through the drive controller itself, which accounts for structural offsets such as tilts and encoder offsets. The RMS pointing accuracy across the sky is estimated at 45 arcseconds. The effect of these pointing errors should be negligible at S-band, and appear as a gain loss of $\leq 1\%$ at X-band.

Lastly, we note that the performance in terms of telescope sensitivity and pointing is the same at the Katherine and Yarragadee sites.

5.2 Baseline lengths and antenna positions

Global VLBI observations as part of the IVS were used to construct baseline length and antenna position time series. The VLBI data were processed using the OCCAM software which adopts the least squares collocation technique (Titov *et al.* 2004). Calculations were performed with respect to the ITRF2005 frame (Altamimi *et al.* 2007), enabling comparisons with independent GPS positions. The Vienna Mapping Function (VMF1, Böhm *et al.* 2006) was implemented, and the analysis carried out according to the IERS 2010 Conventions (Petit and Luzum 2010) with respect to Earth orientation, solid tide, ocean loading, pole tide (including the mean pole model) and thermal expansion. The only exception is for tidal atmospheric loading which has not been included. The celestial reference frame was fixed by the ICRF2 radio source positions with the exception of 39 special handling radio sources (Fey

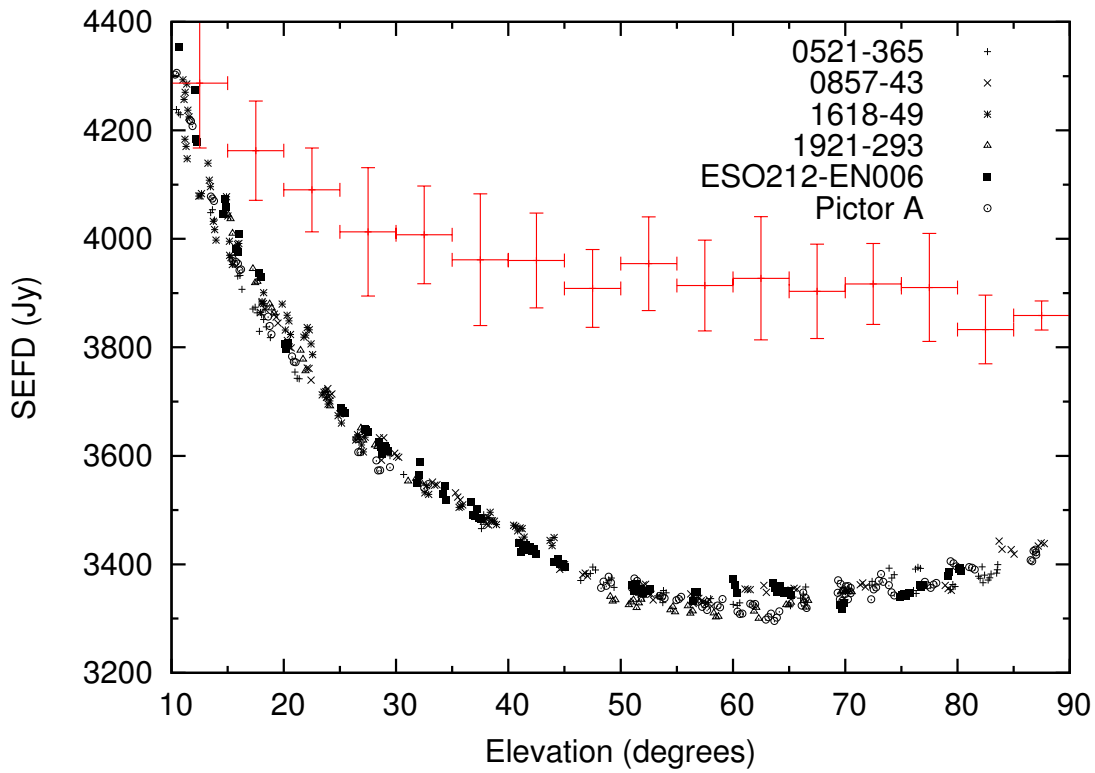


Fig. 5 Measured Hobart 12m System Equivalent Flux Density at both S-band (red crosses) and X-band (black points) as a function of elevation. The S-band measurements have been averaged by bin, as they are somewhat noisier due to terrestrial interference.

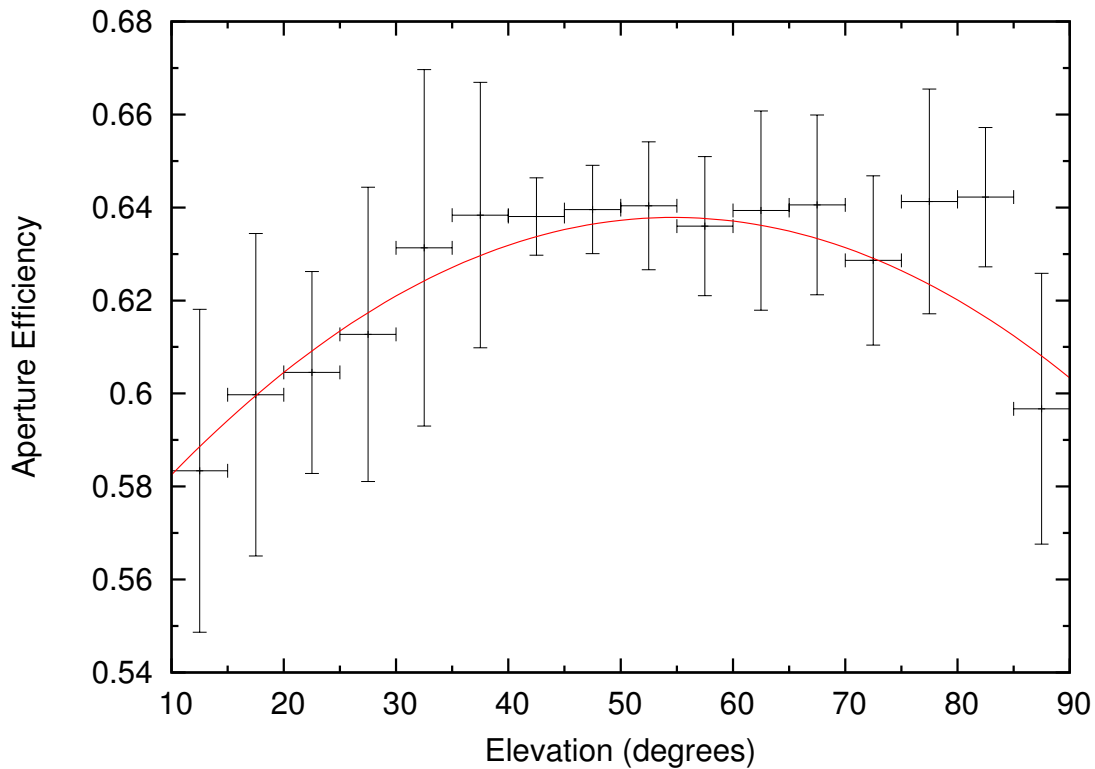


Fig. 6 Hobart 12m aperture efficiency at X-band as a function of elevation

et al. 2009). The geometric delay and gravitational delay models are also based on IERS 2010 Conventions (see Kopeikin 1990; Eubanks 1991; Soffel *et al.* 1991, for details).

A total of 82 daily sessions that included the Hobart 12 m (Hb) antenna were used for this analysis. These sessions comprised IVS Rapid (R1 and R4) experiments which are designed for determination of EOPs, and regional AuScope three-station experiments, scheduled for the purposes of densifying the time-series of solutions for the AuScope antennas and for monitoring and improving the catalogue of southern hemisphere reference radio sources. For R1 and R4 sessions, the coordinates of well-established stations were used to impose the No Net Rotation (NNR) and No Net Translation (NNT) constraints to separate the EOP and geodetic parameters. The positions of the new (AuScope) stations were not constrained. However, it was found that this analysis mode was inappropriate for the regional AuScope sessions. Therefore, for those sessions we decided to first tie the Hb position to ITRF2005, and then add this station position to the list of constraints. During the first run, the Hb position was not included in the NNR and NNT constraints. After preliminary estimation of the Cartesian components, we made a second adjustment imposing NNR and NNT constraints for Hb. The time series for Katherine (Ke) and Yarragadee (Yg) comprised 24 and 14 points respectively. Due to small number statistics, we did not impose the NNR and NNT constraints for these stations.

5.2.1 Baselines and systematic errors

Baseline length repeatability is a fundamental measure of the precision of the VLBI technique. In Figure 7 we show residuals for a typical long baseline between Hb and Kokee Park, Hawaii (Kk) (~ 8300 km). Kokee Park is a reliable VLBI station with a large number of common observations with Hobart. With reference to Figure 7, the two sets of points represent different observing campaigns. Filled points represent the CONT11 campaign, an intensive 15-day set of observations involving the same 14 stations at double the usual recording rate (2 bit sampling rather than 1 bit, giving a 38% improvement in signal-to-noise (Walker 1995)). This is the most comprehensive and homogeneous (in terms of observing strategy) data set available. Open points are standard IVS observations (mostly the Rapid sessions), made with a range of different networks and schedules.

The weighted RMS (WRMS) for the Hb – Kk baseline length during the CONT11 campaign is 0.010 m; this is also the value of the median uncertainty in an individual 24 h measurement. This suggests centimetre

accuracy in position measurements is achievable even with present techniques. By comparison, in Figure 8 we show the same baseline residuals for all available observations (open points). The WRMS is 0.021 m, and median formal uncertainty 0.017 m.

Our results highlight an important point. While formal uncertainties in station positions and baseline lengths can be reduced by increasing the number of observations (since $\sigma \propto N^{-1/2}$), this is not particularly useful when attempting to assess the quality of an individual position measurement. It is clear from Figures 7 and 8 that the main factor at present limiting the accuracy of VLBI observations lies in systematic biases inherent to the analysis. For example, ignorance of quasar structure and variability (which can exhibit different temporal behaviour at S and X bands; e.g. Shabala *et al.* 2012) will map into source and station positions. Furthermore, the magnitude and sign of these effects will in fact depend in a complicated fashion on network geometry and the observing schedule. Charlot and collaborators (e.g. Charlot 1990; Fey and Charlot 1997; Tornatore and Charlot 2007) have shown that group delays due to quasar structure of as much as 1 nanosecond (corresponding to a 30 cm position shift) are possible in individual quasars.

Using the structure index (Fey and Charlot 1997) distribution of ICRF2 quasars (see Figure 12 of Ma *et al.* 2009) and the typical number of observations for each of these quasars, Shabala *et al.* (2013) have calculated the uncertainty in the average group delay due to source structure. These authors find that this value corresponds to position uncertainties of 2.4 cm in the southern hemisphere, and 1.6 cm in the northern hemisphere. They note that the exact value is a strong function of the quasar selection strategy. The distribution of antennas in a network, and time of observation, are important since it is the source structure projected onto a given baseline that determines the additional time delay. Detailed simulations of IVS observations incorporating quasar structure will help address this issue more quantitatively.

We illustrate the significance of systematic errors in Table 2, where we assess the statistical significance of observed weighted RMS (WRMS) for each set of measurements presented in this Section. We have run Monte-Carlo simulations for each set of observations, and calculated the probability of obtaining the observed WRMS by chance. For Hb – Kk observations made in the “normal” mode, the WRMS is significantly different (at the 95 percent level) from the observed formal errors. In other words, the scatter is too large to be due to random scatter alone. On the other hand, the WRMS and formal uncertainties are consistent with each other

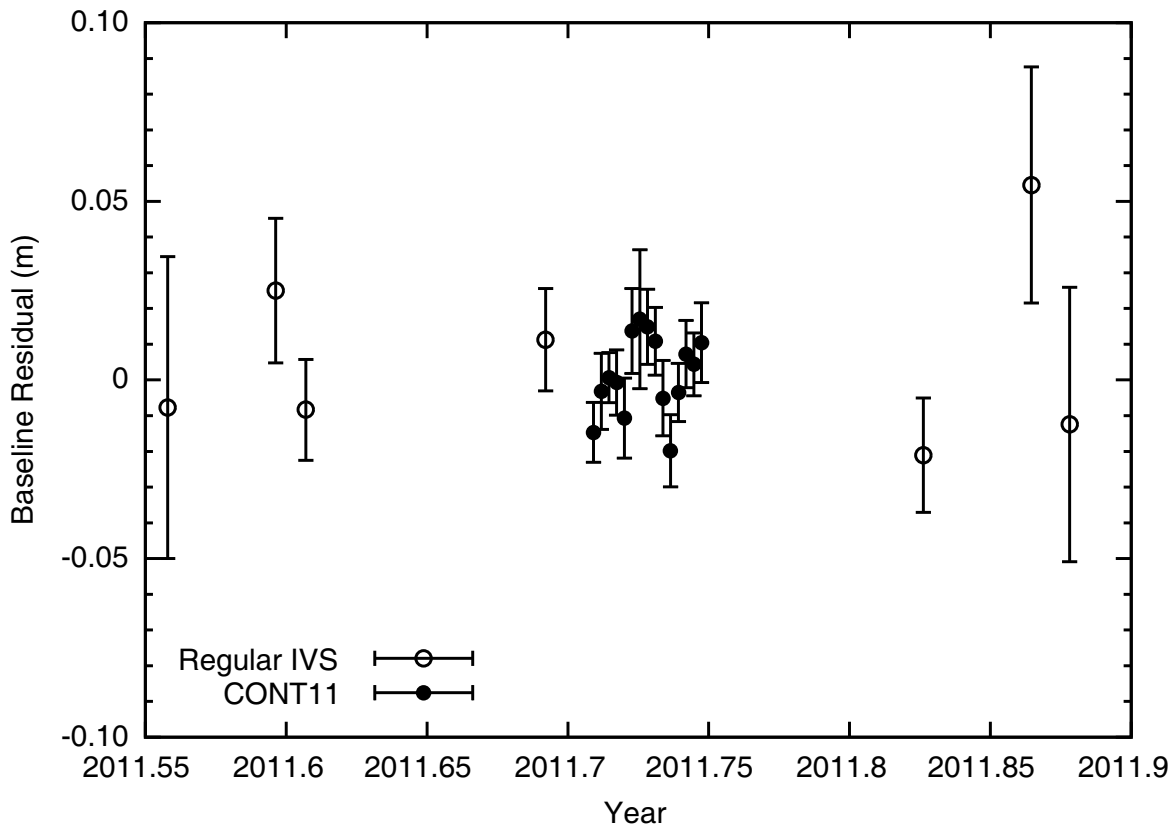


Fig. 7 Time series for residuals for the Hobart 12 m – Kokee (Hb – Kk) baseline. Filled circles represent data from the CONT11 campaign. Open circles are standard IVS sessions.

Table 2 Baseline length repeatability. Observed scatter (WRMS), formal uncertainties (σ) in baseline measurements, and number of observations are shown in the first three columns. WRMS expected from Monte-Carlo simulations, and probability of observed WRMS being consistent with formal uncertainties are shown in the last two columns.

| Baseline | σ (m) | observed WRMS (m) | No. sessions | expected WRMS (m) | prob(WRMS $-\sigma$) |
|------------------------------------------|--------------|----------------------|--------------|----------------------|-----------------------|
| Hobart26 (Ho) – Kokee (Kk), no AuScope | 0.012 | 0.016 | 75 | 0.010 | 0.0001 |
| Hobart26 (Ho) – Kokee (Kk), with AuScope | 0.028 | 0.031 | 17 | 0.025 | 0.097 |
| Hobart12 (Hb) – Kokee (Kk), no CONT11 | 0.022 | 0.0238 | 45 | 0.0201 | 0.064 |
| Hobart12 (Hb) – Kokee (Kk), CONT11 only | 0.0104 | 0.0107 | 15 | 0.0100 | 0.348 |
| Hobart12 (Hb) – Hobart26 (Ho) | 0.0081 | 0.0076 | 22 | 0.0073 | 0.381 |

for the same baseline observed as part of the CONT11 campaign.

We note that the WRMS on the Hb – Kk baseline halves from 0.021 m during regular IVS sessions to 0.010 m for the 15 days of CONT11 observations. These observations were made with an array of the same 14 antennas and the same source catalogue for every session. A marked improvement in baseline length repeatability is achieved, despite the fact that different observing schedules were used for each session, potentially introducing different atmospheric and quasar structure biases into solutions (although the number of observations of a given source per session was roughly constant). This result indicates the important role that network geometry also plays in systematic errors and

emphasises the need for further simulations and observations to disentangle and quantify the error contribution from these two effects.

Also shown in Figure 8 is the Hobart26 (Ho) – Kokee Park baseline, before (black points) and after (grey filled points) the construction of the AuScope array. Inclusion of AuScope antennas is expected to improve both the formal errors on individual sessions, and repeatability (WRMS) of the Ho – Kk baseline. We obtain $(\sigma, \text{WRMS}) = (0.012, 0.016)$ m for the period 2009 – 2010 when no AuScope antennas were involved; and $(0.028, 0.031)$ m in 2011–2012, when AuScope antennas are included. The pre-AuScope RMS is inconsistent with σ at the 99.9 percent level (Table 2) again suggesting systematic sources of position error. Due to higher

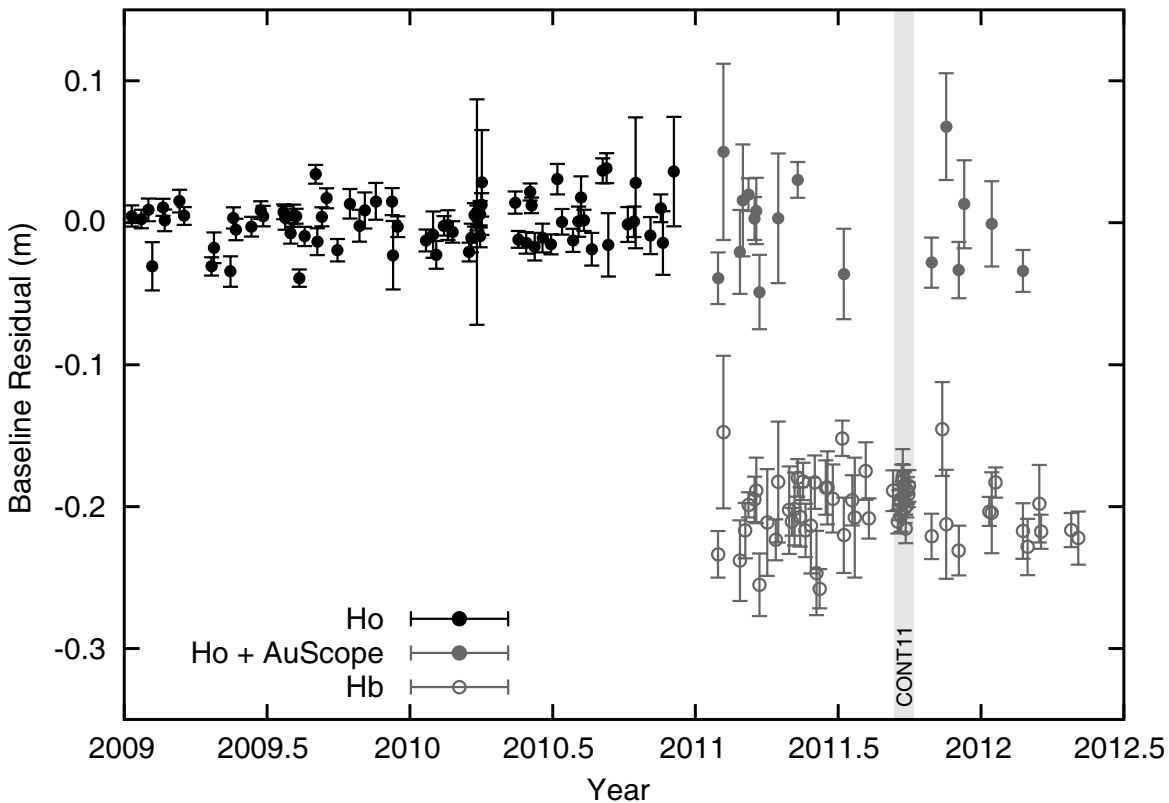


Fig. 8 Time series for residuals for the baselines Hobart 26 m – Kokee (Ho – Kk), and Hobart 12 m – Kokee (Hb – Kk). Black filled circles represent data for the Ho – Kk baseline before construction of AuScope antennas. Grey filled points show the Ho– Kk baseline on days when at least one AuScope station also participated. Grey open points show the Hb – Kk baseline, offset by 20 centimetres for clarity. The grey shaded region corresponds to the CONT11 campaign. With the construction and operation of the AuScope array, Ho has only been observing once per month on average in 2011.

formal errors, the post-AuScope WRMS and σ do not differ in a statistically significant way. The formal errors increase due to Ho being scheduled for a much lower number (a factor of ~ 2) of observations when Hb is included in the schedule. Comparing the velocities of the Ho – Kk and Hb – Kk baselines, we get 0.047 ± 0.003 and $0.059 \pm 0.009 \text{ ma}^{-1}$ respectively. The velocities are consistent within the measured uncertainties. The larger formal baseline errors when AuScope antennas are included are consistent with results for individual antenna positions (Tables 3 and 4). This, in turn, is caused by teething problems during early commissioning at the stations, such as for example frequent clock discontinuities. Another, more subtle, effect is network geometry. AuScope antennas observe in more Southern Hemisphere-dominated networks than did the Hobart 26 m. The scarcity of short baselines means there are very few sources at high mutual elevation; this affects the quality of atmospheric solutions. Furthermore, quasars at low declinations (below -30°) are much less well studied than their Northern Hemisphere counterparts. Many of them show highly variable positions (see e.g. Figure 33 of Ma *et al.* 2009), presum-

ably due to source structure. These effects all contribute to degrading solutions involving the AuScope antennas.

In Figure 9 we show the evolution of the Hb-Ho baseline, noting that both antennas are located on the same bedrock, separated by ~ 296 m. The mean baseline length is 295.917 m, with $(\sigma, \text{WRMS}) = (0.008, 0.007)$ m. These residuals are due to effects such as thermal and gravitational deformation of the antennas, clock stability, and structure of quasars making up the ICRF. Clock stability is an issue here because Ho and Hb currently run off independent time and frequency standards and source structure plays a role as the Ho–Hb baseline measurements were made as part of a global solution. The measured baseline length is in agreement with the results of the Mt. Pleasant local tie survey (Ruddick and Woods 2012) of 295.918 ± 0.001 m. It is interesting that individual station positions (Table 4) agree less well with the local tie survey than the baseline length. This is consistent with errors in individual solution components mapping into estimates of other components (Nothnagel *et al.* 2002).

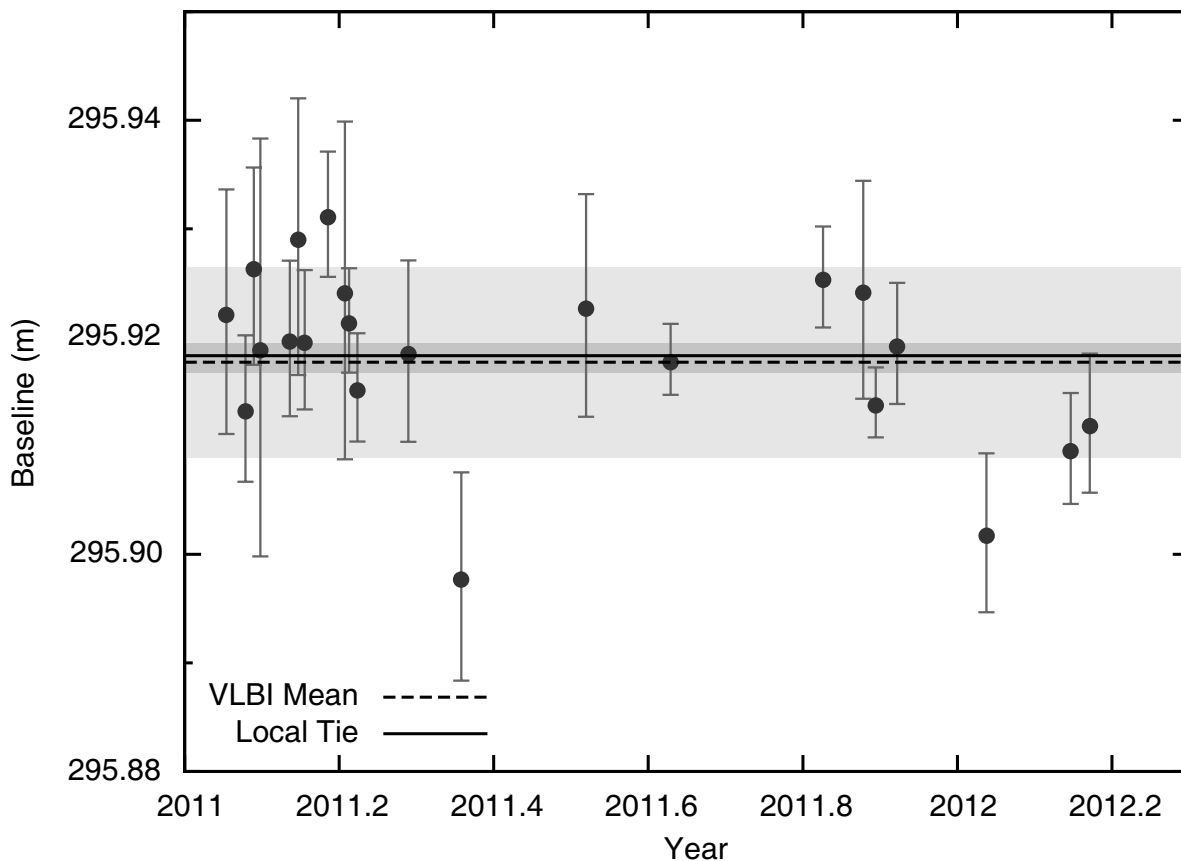


Fig. 9 Time series for the Ho-Hb baseline. The mean baseline length is shown by the dashed line. Results of the local tie survey are shown by the solid black line. Shaded regions are WRMS on the VLBI mean (light grey), and uncertainty in local tie measurement (dark grey).

5.2.2 Antenna positions

Station positions derived from these observations are presented in Tables 3 and 4. Also shown are the station velocities for the Hobart antenna. In Table 3 the inner uncertainties represent the average RMS of individual measurements; while the outer uncertainties denote scatter in best-estimates (i.e. WRMS about the trend line). In other words, the first number corresponds to formal uncertainty given by an OCCAM solution for a typical 24 h session. The second number indicates how repeatable the station position or velocity estimate is from one session to the next. We also quote results of the local tie survey for the Hobart antennas (Ruddick and Woods 2012). In geodetic VLBI, formal uncertainties in baseline lengths and station positions are usually represented via the WRMS (our second set of uncertainties) divided by \sqrt{N} , where N is the number of observations. However, in light of the systematic effects discussed above, which we believe dominate VLBI measurements, we refrain from quoting such overly optimistic values.

6 Conclusions

We have constructed, commissioned and are now operating three new 12m radio telescopes for geodetic VLBI on the Australian continent. We have also constructed and tested a new software correlator facility for geodesy at Curtin University. For the observatories, we have followed a design strategy to match the VLBI2010 requirements as closely as possible and to allow an upgrade to full VLBI2010 capabilities in the future. All three telescopes are operated remotely with a high level of reliability. The individual telescopes are meeting their design specifications in terms of mechanical performance and sensitivity. As elements of a VLBI array we have demonstrated their capability to achieve centimetre precision in typical baseline measurements and have presented non-variant point positions for all three telescopes.

Data taken during the 15 day CONT11 campaign have shown the dramatic improvement to positional accuracy and repeatability that can be achieved by observations with a non-varying global array of telescopes. We suggest that further reductions in systematic errors

Table 3 Calculated positions for the three AuScope VLBI antennas at epoch 2012.0, ITRF2005 datum. The first uncertainty represents the average formal error in an individual measurement. The second uncertainty corresponds to weighted scatter about the best estimate.

| Hobart 12 m (Hb) | |
|----------------------|-----------------------------------------|
| No. Sessions | 82 |
| Latitude (d m s) | $-42\ 48\ 20.0621 \pm (0.0006, 0.0012)$ |
| Longitude (d m s) | $147\ 26\ 17.3070 \pm (0.0006, 0.0012)$ |
| Height (m) | $40.967 \pm (0.019, 0.036)$ |
| Katherine 12 m (Ke) | |
| No. Sessions | 24 |
| Latitude (d m s) | $-14\ 22\ 31.6679 \pm (0.0006, 0.0004)$ |
| Longitude (d m s) | $132\ 09\ 08.5439 \pm (0.0007, 0.0006)$ |
| Height (m) | $189.262 \pm (0.021, 0.017)$ |
| Yarragadee 12 m (Yg) | |
| No. Sessions | 14 |
| Latitude (d m s) | $-29\ 02\ 49.7226 \pm (0.0012, 0.0006)$ |
| Longitude (d m s) | $115\ 20\ 44.2576 \pm (0.0013, 0.0013)$ |
| Height (m) | $248.236 \pm (0.040, 0.029)$ |

Table 4 Calculated positions for the three AuScope VLBI antennas and Hobart26, and Hobart12 velocities at epoch 2009.9 in geodetic coordinates, ITRF2005 datum. Quoted uncertainties are WRMS values. Local tie survey results of Ruddick and Woods (2012) for the Hobart antennas are also shown.

| Station | X (m) | Y (m) | Z (m) |
|---------------------------------------------|---------------------------|--------------------------|---------------------------|
| Hobart26 (Ho) VLBI | -3950237.247 ± 0.013 | 2522347.670 ± 0.008 | -4311562.033 ± 0.018 |
| Hobart26 (Ho) local tie | -3950237.251 ± 0.0006 | 2522347.669 ± 0.0003 | -4311562.015 ± 0.0004 |
| Hobart12 (Hb) VLBI | -3949990.687 ± 0.044 | 2522421.191 ± 0.012 | -4311708.164 ± 0.032 |
| Hobart12 (Hb) local tie | -3949990.676 ± 0.0004 | 2522421.199 ± 0.0003 | -4311708.170 ± 0.0003 |
| Hobart12 (Hb) velocity (ma^{-1}) | -0.038 ± 0.009 | -0.001 ± 0.004 | 0.046 ± 0.007 |
| Katherine (Ke) VLBI | -4147354.453 ± 0.018 | 4581542.384 ± 0.017 | -1573303.310 ± 0.012 |
| Yarragadee (Yg) VLBI | -2388896.040 ± 0.036 | 5043349.973 ± 0.029 | -3078590.989 ± 0.015 |

can be made by careful selection of radio sources and by comparing observations made using suitable quasars with different schedules. Investigation of these effects is being undertaken through the AUSTRAL observing program within the IVS which is using the three AuScope telescopes and the near-identical 12 m telescope at Warkworth, New Zealand (Gulyaev and Natusch 2010). These observations are being undertaken to strengthen the Southern Hemisphere reference frame and to exercise the full capabilities of these small, fast antennas with high data recording rates, which allow for typically twice the number of observations per telescope per day as the IVS Rapid observations. The improved observation rate, constant array configuration, judicious source selection and scheduling is expected to further reduce systematic errors. We are also using surveying techniques to study the thermally and gravitationally induced deformation of the 12 m telescopes in order to quantify and subsequently mitigate this systematic effect.

The most important upgrade now required to the AuScope VLBI array is a $\sim 2 - 14$ GHz broadband receiving and recording system to bring it significantly closer to the ultimate VLBI2010 aim of millimetre accurate positions.

Acknowledgements This study made use of data collected through the AuScope initiative. AuScope Ltd is funded under the National Collaborative Research Infrastructure Strategy (NCRIS), an Australian Commonwealth Government Programme. JM and SS were supported under the Australian Research Council’s Super Science funding scheme (projects FS110200045 and FS100100037). We wish to thank our Reviewers for a comprehensive and constructive list of comments. Lastly we wish to thank the International VLBI Service for Geodesy and Astrometry (IVS) for access to VLBI data products used in this paper and for advice and support during the conception, design, commissioning and operation of the AuScope VLBI Array.

References

- Altamimi, Z., Collilieux, X., Legrand, J., Garayt, B., and Boucher, C. (2007). ITRF2005: A new release of the International Terrestrial Reference Frame based on time series of station positions and Earth Orientation Parameters. *J. Geophys. Res.*, **112**, B09401.
- Altamimi, Z., Collilieux, X., and Métivier, L. (2011). ITRF2008: an improved solution of the international terrestrial reference frame. *Journal of Geodesy*, **85**, 457–473.
- AuScope (2012). AuScope: An organisation for a national earth science infrastructure program. <http://www.auscope.org.au>.
- Böhm, J., Werl, B., and Schuh, H. (2006). Troposphere mapping functions for GPS and very long baseline interferometry from European Centre for Medium-Range Weather

- Forecasts operational analysis data. *J. Geophys. Res.*, **111**, B02406.
- Charlot, P. (1990). Radio-source structure in astrometric and geodetic very long baseline interferometry. *AJ*, **99**, 1309–1326.
- Deller, A. T., Tingay, S. J., Bailes, M., and West, C. (2007). DiFX: A Software Correlator for Very Long Baseline Interferometry Using Multiprocessor Computing Environments. *PASP*, **119**, 318–336.
- Deller, A. T., Briskin, W. F., Phillips, C. J., Morgan, J., Alef, W., Cappallo, R., Middelberg, E., Romney, J., Rottmann, H., Tingay, S. J., and Wayth, R. (2011). DiFX-2: A More Flexible, Efficient, Robust, and Powerful Software Correlator. *PASP*, **123**, 275–287.
- Eubanks, T. M. (1991). A Consensus Model For Relativistic Effects In Geodetic VLBI. In T. M. Eubanks, editor, *Proceedings Of The U.S. Naval Observatory Workshop On Relativistic Models For Use In Space Geodesy*, pages 60–82. U. S. Naval Observatory.
- Fey, A. L. and Charlot, P. (1997). VLBA Observations of Radio Reference Frame Sources. II. Astrometric Suitability Based on Observed Structure. *ApJS*, **111**, 95.
- Fey, A. L., Gordon, D., and Jacobs, C. S. (2009). The Second Realization of the International Celestial Reference Frame by Very Long Baseline Interferometry. *IERS Technical Note*, **35**.
- Gatti, M. S. (2004). The Deep Space Network Large Array. Technical Report 42–157, Jet Propulsion Laboratory, California.
- Gulyaev, S. and Natusch, T. (2010). New Zealand 12 m VLBI Station. In D. Behrend and K. D. Baver, editors, *International VLBI Service for Geodesy and Astrometry 2009 Annual Report*, number NASA/TP 2010-215860, pages 138 – 141.
- Herring, T. A., Mathews, P. M., and Buffett, B. (2002). Modeling of nutation-precession: Very long baseline interferometry results. *J. Geophys. Res.*, **107**, 2069.
- Imbriale, W. A. (2005). Radio Frequency Optics Design of the 12-Meter Antenna for the Array-Based Deep Space Network. *The Interplanetary Network Progress Report*, **42-160**.
- Kettenis, M., van Langevelde, H. J., Reynolds, C., and Cotton, B. (2006). ParselTongue: AIPS Talking Python. In C. Gabriel, C. Arviset, D. Ponz, and S. Enrique, editors, *Astronomical Data Analysis Software and Systems XV*, volume 351 of *Astronomical Society of the Pacific Conference Series*, page 497.
- Kopeikin, S. M. (1990). Theory of Relativity in Observational Radio Astronomy. *Soviet Ast.*, **34**, 5.
- Ma, C., Arias, E. F., Bianco, G., Boboltz, D. A., Bolotin, S. L., Charlot, P., Engelhardt, G., Fey, A. L., Gaume, R. A., Gontier, A.-M., Heinkelmann, R., Jacobs, C. S., Kurdubov, S., Lambert, S. B., Malkin, Z. M., Nothnagel, A., Petrov, L., Skurikhina, E., Sokolova, J. R., Souchay, J., Sovers, O. J., Tesmer, V., Titov, O. A., Wang, G., Zharov, V. E., Barache, C., Boeckmann, S., Collioud, A., Gipson, J. M., Gordon, D., Lytvyn, S. O., MacMillan, D. S., and Ojha, R. (2009). The Second Realization of the International Celestial Reference Frame by Very Long Baseline Interferometry. *IERS Technical Note*, **35**, 1.
- MONICA (2011). open-monica. <http://code.google.com/p/open-monica/>.
- NCRIS (2006). National Collaborative Research Infrastructure Strategy (NCRIS). <http://www.innovation.gov.au/Science/ResearchInfrastructure/Pages/NCRIS.aspx>.
- Neidhardt, A., Ettl, M., Plötz, C., Mühlbauer, M., Hase, H., Sobarzo Guzmán, S., Herrera Ruztort, C., Alef, W., Rottmann, H., and Himwich, E. (2010). Interacting with radio telescopes in real-time during VLBI sessions using e-control. In *Proceedings of the 10th European VLBI Network Symposium and EVN Users Meeting: VLBI and the new generation of radio arrays. September 20-24, 2010. Manchester, UK*.
- Niell, A., Whitney, A., Petrachenko, W., Schlüter, W., Vandenberg, N., Hase, H., Koyama, Y., Ma, C., Schuh, H., and Tuccari, G. (2007). VLBI2010: A Vision for Future Geodetic VLBI. In F. Sanso, editor, *Dynamic Planet - Monitoring and Understanding a Dynamic Planet with Geodetic and Oceanographic Tools*, volume 130, page 757.
- Nothnagel, A., Vennebusch, M., and Campbell, J. (2002). On correlations between parameters in geodetic VLBI data analysis. In N. Vandenberg and K. D. Baver, editors, *IVS 2002 General Meeting Proceedings*, page 260.
- Ott, M., Witzel, A., Quirrenbach, A., Krichbaum, T. P., Standke, K. J., Schalinski, C. J., and Hummel, C. A. (1994). An updated list of radio flux density calibrators. *A&A*, **284**, 331–339.
- Petit, G. and Luzum, B. (2010). IERS Conventions (2010). *IERS Technical Note*, **36**, 179.
- Petrachenko, W. T., Schuh, H., Niell, A. E., Behrend, D., and Corey, B. E. (2010). VLBI2010: Next Generation VLBI System for Geodesy and Astrometry. *AGU Fall Meeting Abstracts*, page B6.
- Ruddick, R. and Woods, A. (2012). The 2009 Mount Pleasant (Hobart) Observational Local Tie Survey. Geoscience Australia Record, in preparation.
- Schuh, H. and Behrend, D. (2012). VLBI: A fascinating technique for geodesy and astrometry. *Journal of Geodynamics*, **61**, 68–80.
- Shabala, S. S., Titov, O., Lovell, J., McCallum, J., Blanchard, J., Watson, C., and Dickey, J. (2012). Quasar structure effects on the VLBI reference frame: the case of 1144–379. *IVS 2012 General Meeting Proceedings*. Submitted.
- Shabala, S. S., Memin, A., and McCallum, J. (2013). Systematic Biases in Geodetic VLBI Analysis. *Publications of the Astronomical Society of Australia*. Submitted.
- Soffel, M. H., Wu, X., Xu, C., and Mueller, J. (1991). Consistent relativistic VLBI theory with picosecond accuracy. *AJ*, **101**, 2306–2310.
- Tingay, S. J., Alef, W., Graham, D., and Deller, A. T. (2009). Geodetic VLBI correlation in software. *J Geod*, **83**(11), 1061 – 1069.
- Titov, O. (2007). Effect of the selection of reference radio sources on geodetic estimates from VLBI observations. *J Geod*, **81**, 455 – 468.
- Titov, O. (2009). A new estimator for VLBI baseline length repeatability. *J Geod*, **83**(11), 1041 – 1049.
- Titov, O., Tesmer, J., and Boehm, J. (2004). OCCAM v6.0 software for VLBI data analysis. In N. Vandenberg and K. Baver, editors, *Proceedings of the 2004 IVS 3rd General Meeting*, page 267.
- Tornatore, V. and Charlot, P. (2007). The impact of radio source structure on European geodetic VLBI measurements. *J Geod*, **81**, 469.
- Walker, R. C. (1995). What the VLBA Can Do for You: Capabilities, Sensitivity, Resolution, and Image Quality. In J. A. Zensus, P. J. Diamond, and P. J. Napier, editors, *Very Long Baseline Interferometry and the VLBA*, volume 82 of *Astronomical Society of the Pacific Conference Series*, pages 133 – 157.